

Renormalization of trajectories with zero quantum numbers in dual unitarization*

Tsou Sheung Tsun[†]

Institute for Theoretical Physics, State University of New York at Stony Brook, Stony Brook, New York 11794

(Received 22 April 1977)

The renormalization of the f , f' , ω , and ϕ trajectories through the crossed-loop (or cylinder) insertion is exhaustively studied in the context of dual unitarization. The trajectory functions $\alpha(t)$, mixing angles, and couplings are obtained for the range $-1.0 \leq t \leq 2.0 \text{ GeV}^2$. In particular, it is found that the f is renormalized upwards by a considerable amount, acquiring an intercept $\alpha_f(0) \simeq 0.93$ and slope $\alpha_f'(0) \simeq 0.4$. It becomes still flatter for $t < 0$. These characteristics, together with its symmetry properties, strongly support its identification with the experimental Pomeron. At the same time, the mass splitting of f and A_2 is correctly given as about 0.1 GeV^2 . The ω trajectory is renormalized downwards, and acquires a considerable admixture of the strange component, in agreement with the phenomenological estimates of $\gamma_{KK}^\omega/\gamma_{KK}^p \simeq 1.4$. Furthermore, the t dependence of the calculated quantities in general verifies the prediction that renormalization effects decrease as t increases.

I. INTRODUCTION

In hadron interactions there are several experimentally deduced regularities such as the exchange degeneracy of Regge trajectories, the ideal mixing of quark states, and the Okubo-Zweig-Iizuka rule for resonance decay. Deviations from these patterns are in general small. Dual unitarization¹⁻³ is a scheme constructed to reproduce such regularities as a first approximation and to calculate deviations from them as higher-order corrections. The most important of these corrections concerns the vacuum trajectory f , which has been studied by many authors^{2,4-12} and which is found to deviate from exchange degeneracy by a considerable amount; the deviation is, furthermore, strongly t dependent. These studies were, however, all done at or very near the forward direction. In this paper we wish to extend these ideas to a larger range of t , both positive and negative, for not only the f trajectory but the other zero-quantum-number trajectories f' , ω , and ϕ . Preliminary results of this study have already been reported elsewhere.¹⁰

Dual unitarization starts with the set of all planar quark diagrams, which preserve the symmetries mentioned above, and derives a bootstrap equation^{2,3,13} restricting the quantities that come into play at this planar level. Let N be the number of quark flavors and let us assume for the moment exact $SU(N)$ symmetry. Then bootstrap gives us the schematic equation

$$\bar{g}^2 N \sim 1, \tag{1}$$

as illustrated in Fig. 1(a), where \bar{g} is some effective coupling constant averaged over the loop. This gives us the value of \bar{g} , which then fixes the scale of higher-order corrections. The ideas of topological expansion¹⁴ are very similar to ours.

The next higher order corresponds to the crossed loop, as illustrated in Fig. 1(b), having the topology of a cylinder.^{14,5} This is a nonplanar diagram. Since the quark lines return they cannot carry any quantum numbers, so that it can only renormalize trajectories with zero quantum numbers (of both signatures), i.e., the f , ω , f' , and ϕ . In principle, other higher-order diagrams, corresponding to more complicated topology, should also be considered when studying the renormalization of these trajectories. However, calculations^{15,16} of the next order diagram in connection with the ρ - A_2 and K^* - K^{**} trajectories show that the splitting is less than 0.1 for the intercepts, whereas as we shall see the crossed loop gives a renormalization of about 0.5 for the intercept of the f . Hence the most significant diagram for the vacuum trajectories is still Fig. 1(b).

There is another very good reason why we want to study exclusively Fig. 1(b) here. It is the only [besides Fig. 1(a)] for which a full three-dimensional formulation has been constructed,^{1,2} and this is necessary if we want to know about not only the intercept, but also the t dependence of the renormalization.

Our calculations show that the f trajectory acquires an intercept of about 0.93, with a small slope of about 0.4 at $t=0$. This is extremely reminiscent of the experimental Pomeron. At the same

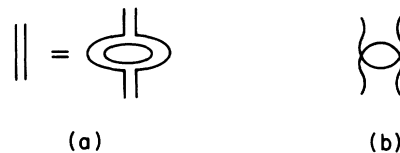


FIG. 1. (a) The bootstrap condition on planar loops. (b) The crossed loop.

time, we obtain the correct f_0 - A_2 mass splitting at the resonance position. Further comparison of predicted couplings with data strengthens the f -Pomeron identity in this model. The ω trajectory is renormalized downwards and acquires a considerable mixture of the $\lambda\bar{\lambda}$ component. In general, our renormalized trajectories attest to the prediction that renormalization effects decrease as t increases.^{5,17} Some results for the secondary trajectories f' and ϕ are also obtained. Besides trajectory functions, we have also calculated Regge couplings and mixing angles, all in fair agreement with experiment wherever comparison is possible.

II. THE CROSSED-LOOP INSERTION

For definiteness, let us take the case $N = 3$. We shall consider $SU(3)$ symmetry breaking only to the extent that the λ quark is heavier than the normal quarks $\mathcal{N} = \mathcal{P}$. In principle, we can incorporate charm. However, the charmed quark is supposed to be even heavier than λ and is hence much more difficult to excite. Its inclusion will therefore have very little effect on the high-lying trajectories that we are interested in.

Before any nonplanar diagrams are introduced, Regge trajectories are exchange degenerate and the quark states do not mix. This means that we have, to start with, three distinct exchange degenerate trajectories. The crossed-loop insertion will mix states, but since it cannot carry any quantum numbers, only trajectories with zero quantum numbers will be affected. Let us represent the planar ("unrenormalized") Regge propagator by the matrix P , and the crossed-loop kernel by the matrix C , as in Fig. 2. Notice that P is diagonal.

In contrast to the uncrossed loop [Fig. 1(a)], which has one free quark loop and so is formally of order $\bar{g}^2 N \sim 1$, the crossed loop [Fig. 1(b)] is of order \bar{g}^2 .^{7,10} However, if we iterate the crossed loop n times (Fig. 3), we still get an order of \bar{g}^2 , since $\bar{g}^2(\bar{g}^2 N)^{n-1} \sim \bar{g}^2$ by (1). Hence when we consider the crossed-loop insertion, we have to in-

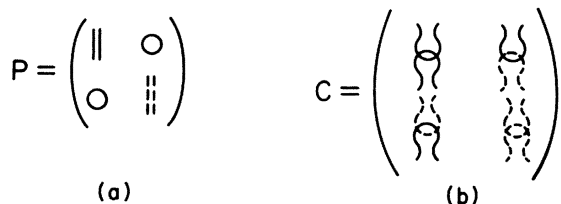


FIG. 2. (a) The unrenormalized propagator, and (b) the crossed-loop kernel, both in matrix notation, where solid lines represent the normal \mathcal{N} , \mathcal{P} quarks and dotted lines represent the strange quark λ .

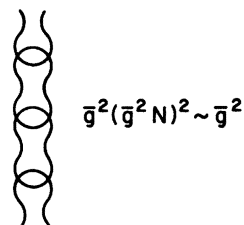


FIG. 3. A chain of crossed loops.

clude its iteration to infinitely many times as well. Notice, however, that because of the direction of the quark lines, iterations with an even number of loops have positive sign for both signatures, while iterations with an odd number of loops have positive sign for even and negative sign for odd signatures.⁷ Hence if we denote by P'_+ and P'_- the renormalized propagators for $\sigma = \pm$, we have

$$P'_\pm = P \pm PCP + PCPCP \pm PCPCPCP + \dots \quad (2)$$

Because the elements of C are all positive, this means that the f and f' trajectories will be renormalized upwards and the ω and ϕ downwards.

III. THE SUM OF CROSSED LOOPS

Equation (2) tells us only schematically that we have to calculate chains of crossed loops such as in Fig. 3. In order to obtain the renormalized Regge propagators we need a more concrete model. In an earlier work,^{1,2} a formula based on Regge asymptotic behavior and semilocal duality was written for the imaginary part of the n -loop amplitude for $SU(N)$ symmetry. It is readily generalized to our case of broken $SU(3)$ and different input trajectories.

Since we are considering only two distinct types of quarks, we have, to start with, three trajectories corresponding to the states

- (i) $(1/\sqrt{2})(\mathcal{N}\bar{\mathcal{N}} + \mathcal{P}\bar{\mathcal{P}})$: α_{11} , which we call the " ρ trajectory" for convenience,
- (ii) $\mathcal{N}\bar{\lambda}$, $\mathcal{P}\bar{\lambda}$ and $\bar{\mathcal{N}}\lambda$, $\bar{\mathcal{P}}\lambda$: α_{12} and α_{21} , or the " K^* trajectory," and
- (iii) $\lambda\bar{\lambda}$: α_{22} , or the " ϕ trajectory."

We assume them to be linear, but not necessarily with a universal slope:

$$\alpha_{ij}(t) = \alpha_{ij}^0 + \alpha'_{ij}t, \quad i, j = 1, 2. \quad (3)$$

Next let $V(t; t_1, t'_1)$ denote the triple-Regge vertex (Fig. 4), where the t 's are momentum transfers as indicated. Following Ref. 2 we represent its rapid cutoff at large t_1 and t'_1 by a factor similar to the Veneziano beta function, and the rest of the various t dependences by exponentials. We thus write

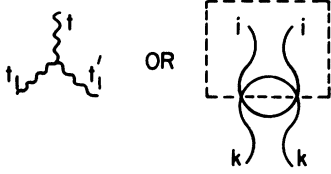


FIG. 4. Variables appearing in the triple-Regge vertex.

$$V(t; t_1, t'_1) = g^2(1 - Rt_1)^{t_1}(1 - Rt'_1)^{t'_1} \times \exp[\alpha'_{ik}\kappa(t) + \alpha'_{ik}\mu(t_1, t'_1)], \quad (4)$$

where $R = 4/e$ and g is the coupling constant. Besides giving the value of g the planar bootstrap

$$(I_n(s, t))_{i,j} = \sum_k \int_0^\infty ds_1 s_1^{-2\alpha'_{ik}} F(s, s_1, t)_{ik} (I_{n-1}(s_1, t))_{kj}, \quad (5)$$

where

$$(F(s, s_1, t))_{ik} = W(i, k) \int_0^{\sqrt{s-\sqrt{s_1}}} ds_2 \left(\frac{s}{s_2}\right)^{2\alpha'_{ik}} s_2^{\alpha'_{ii}} s_2'^{\alpha'_{ii}} (H(s, s_1, s_2, t))_{ik},$$

$$(H(s, s_1, s_2, t))_{ik} = \frac{g^2 N}{8\pi^3} \frac{1}{s} \frac{1}{\alpha'_{ik} a} \exp(2\alpha'_{ik} a t_{\min}) \{1 - \exp[-2\alpha'_{ik} a (\lambda\lambda')^{1/2}/s]\} \exp[\frac{1}{2}\alpha'_{ik} a t (\lambda'/\lambda)^{1/2} + \alpha'_{ii}\kappa(t)],$$

$$a = \ln\left(\frac{s'}{s_1 s_2'} + R\right), \quad s' = s + C, \quad s_1' = s_1 + C, \quad s_2' = s_2 + C,$$

$$\lambda = \lambda(s_1, 0, 0), \quad \lambda' = \lambda(s, s_1, s_2),$$

$$t_{\min} = \frac{1}{2s} [-\lambda^*(s, s, 0, s_1, 0, s_2) + (\lambda\lambda')^{1/2}],$$

$$W(i, k) = \begin{pmatrix} 2 & \sqrt{2} \\ \sqrt{2} & 1 \end{pmatrix},$$

and the indices i, j are not summed. The matrix W takes account of the fact that there are two normal quarks to one strange quark. For detailed explanation of the other symbols the reader is referred to Eqs. (14) to (24) of Ref. 2. We note that the n -loop amplitude is given in a recursion relation which greatly simplifies the summation of the different loops.

Equation (5) was to represent the imaginary part of the n -loop amplitude for a physical process, so that we should put in external couplings and in general nonzero external masses. However, since we are now interested in Eq. (5) as representing a renormalized Regge propagator, by factorization we can leave out the external couplings and then the value of the external masses is irrelevant.¹⁸

To get the imaginary part of the amplitude, we sum up the loops:

$$(I^+(s, t))_{i,j} = \sum_{n=0}^{\infty} (I_n(s, t))_{i,j}. \quad (6)$$

equation² determines one more parameter among the functions $\kappa(t)$ and $\mu(t_1, t'_1)$. The function $\mu(t_1, t'_1)$ is more amenable to comparison with experiment. In fact, an analysis with data² shows that if we write $\mu(t_1, t'_1) = \mu_0(t_1 + t'_1)$, then μ_0 is consistent with the value 0. So only the function $\kappa(t)$ remains. This will be discussed in the next section.

With these modifications in mind, the formula for the imaginary part of the n -loop amplitude can be rewritten as follows:

$$(I_0(s, t))_{i,j} = \delta_{ij} s^{\alpha'_{ij}} s'^{\alpha'_{ij} t}$$

and for $n > 0$,

For the symmetric case, it was found² that (6) had Regge behavior at high energies. In the case of broken SU(3), we have to work a bit harder because we want to extract information not only for the leading trajectory but also for the next-to-leading one. Now although there are only two poles in the input, we cannot expect not to generate new singularities after renormalization. It is only in very simplified cases, for example, with a constant kernel C^5 , that this can be true. A simple j dependence in C already produces extra low-lying complex poles.⁴ Our more realistic representation of C is sure to give a richer structure in the space of the output states. In particular, the two highest-lying output poles do not in general constitute a complete set of states. There may be daughters, complex poles, and even cuts. In terms of mixing this means that the angles representing mixing will in general be j dependent. This is in contrast to the normal usage for mixing angles. However, the use of angles to describe mixing is still con-

venient in our formalism.

Hence, if we are interested only in the two highest-lying poles, we can write for the matrix elements asymptotically

$$\begin{aligned} (I^*(s, t))_{11} &= \beta_f^2(t) \cos^2 \theta_f(t) s^{\alpha_f(t)} \\ &\quad + \beta_{f'}^2(t) \sin^2 \theta_{f'}(t) s^{\alpha_{f'}(t)}, \\ (I^*(s, t))_{12} &= (I^*(s, t))_{21} \\ &= \beta_f^2(t) \cos \theta_f(t) \sin \theta_f(t) s^{\alpha_f(t)} \\ &\quad + \beta_{f'}^2(t) \cos \theta_{f'}(t) \sin \theta_{f'}(t) s^{\alpha_{f'}(t)}, \\ (I^*(s, t))_{22} &= \beta_f^2(t) \sin^2 \theta_f(t) s^{\alpha_f(t)} \\ &\quad + \beta_{f'}^2(t) \cos^2 \theta_{f'}(t) s^{\alpha_{f'}(t)}. \end{aligned} \quad (7)$$

The β 's are ratios of the couplings of the renormalized to the input trajectories, and θ_f is not necessarily equal to $\theta_{f'}$.

For odd signature, we take alternating signs in the summation [cf. Eq. (2)],

$$(I^*(s, t))_{i,j} = \sum_{n=0}^{\infty} (-1)^n (I_n(s, t))_{i,j}, \quad (8)$$

with the matrix elements corresponding to ω and ϕ as the two highest output trajectories, in exact analogy to (7). Here we call the highest lying $\sigma = -$ trajectory ω , and the next-to-leading ϕ . Whether they actually correspond to the ω and ϕ mesons remains to be seen.

IV. CALCULATIONS AND RESULTS

First of all we shall fix the input trajectories. To do this we make use of the fact that nonvacuum trajectories are not affected by the crossed loop and consequently only very slightly by the other higher diagrams. This means that we can take their experimental values as their bare values without appreciable error. Linear interpolation and extrapolation of the Chew-Frautschi plot then give us

$$\begin{aligned} \alpha_{11}(t) &= 0.5 + 0.85t, \\ \alpha_{12}(t) &= \alpha_{21}(t) = 0.35 + 0.81t, \\ \alpha_{22}(t) &= 0.2 + 0.77t, \end{aligned} \quad (9)$$

following the parameterization of Eq. (3). The last trajectory is obtained assuming the Gell-Mann-Okubo rule for both the intercepts and slopes.¹⁹ On the Chew-Frautschi plot one sees that $\alpha_{22}(t)$ actually passes through the physical ϕ and f' . The smallness of the renormalization of f' , which we obtain later, partly justifies this, although we are unsure of the renormalization of the ϕ for reasons we shall discuss.

Next we turn to the planar bootstrap for fixing the triple-Regge vertex. Now the planar boot-

strap² gives

$$g^2 N \simeq 150 \quad (10)$$

for SU(N) symmetry. In principle we can do a similar bootstrap for broken SU(N). In practice, however, because of the difficulties in formulating rigorously the bootstrap condition, this is neither feasible nor profitable. Furthermore, since the heavier quarks are progressively more difficult to excite, it is reasonable to substitute for N an N_{eff} while keeping the bootstrapped value for the product $g^2 N_{\text{eff}}$. Using a suppression factor for the λ quark derived from experiment Papadopoulos *et al.*⁶ gives the estimate

$$2 \leq N_{\text{eff}} \leq 2.5.$$

They also find that the effect of charm is negligible. At the same time, Dodd²¹ obtains in a simplified model calculation

$$N_{\text{eff}} \simeq 2.3 \quad (11)$$

when he considers broken SU(4). This is a reasonable value to use in our case, considering the conclusions of Papadopoulos *et al.* Equations (10) and (11) then give

$$g \simeq 8.0. \quad (12)$$

The last input we need to specify is the t dependence of the triple-Regge vertex, which was left as $\kappa(t)$ in Eq. (5). The restricted small- t region we are considering justifies the use of exponentials in $V(t, t_1, t_1')$. Now if we further assume

$$\kappa(t) = \kappa_0 t \quad (13)$$

as in Ref. 2, then the bootstrap gives

$$\kappa_0 = -0.9. \quad (14)$$

Most of our calculations are done with this parameterization and the results compare quite favorably with data as we shall see. However, (13) and (14) cannot be entirely satisfactory because they give a slightly curved output trajectory in the bootstrap once we take t away from zero. This means that V should have a stronger t dependence. In principle one can do a planar bootstrap at every (small) value of t and thus obtain the exact t dependence of V . Unfortunately the particular form of the bootstrap equation adopted in Ref. 2 is not suitable for this and does not give sensible results away from $t=0$. So if we insist on improving (13) and (14), we have to resort to data-fitting, for example with the f_0 mass as detailed at the end of this section. Although the addition of a quadratic term in (13) would give a stronger t dependence to V as desired, it is unsatisfactory for $t < 0$, where the renormalization would be too small. Hence we shall still keep the linear form (13) and only vary

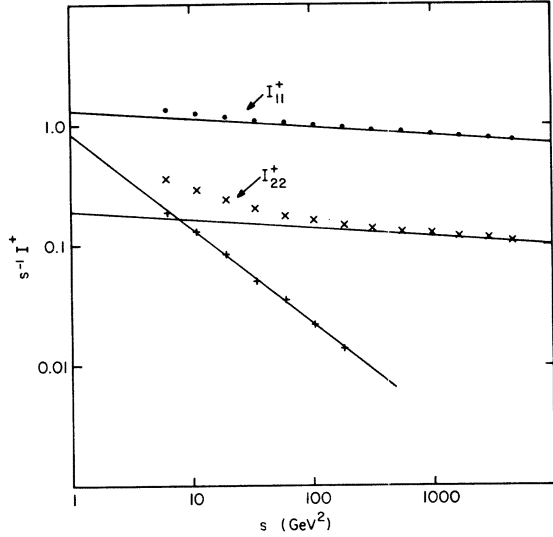


FIG. 5. I_{11}^+/s and I_{22}^+/s as functions of s , plotted at $t=0$. The straight lines correspond to the asymptotic power behaviors giving α_f and $\alpha_{f'}$ (see text).

(14) when fitting with the f_0 mass.

All the other parameters that occur in Eq. (5) are fixed as in Refs. 2 and 10.

Equations (6) and (8) were evaluated numerically up to asymptotic energies in the small range of $-1.0 \leq t \leq 2.3$. Our aim is to get to high enough energy for (7) to hold, so that we can extract from it the Regge parameters of interest. In contrast to the symmetric case,¹⁰ energy has to be high enough for both diagonal terms in (7) to reach Regge behavior. For negative t and very small positive t , we find that calculating up to $s \sim 5000$ GeV^2 is enough for our purpose. For larger $t > 0$ we evaluated the formulas up to $s \sim 50000$ GeV^2 . We need higher energy here because the angle θ_f (and θ_{ω}) becomes smaller as t increases, so that it takes a longer time for the first term in I_{22} to win over the second.

The number of loops required for a given energy depends on that energy because higher loops have higher energy thresholds. It also depends on the t region. In general for even signature, where all loops are added with a positive sign, we find that summing up to $n=11$ is sufficient. This value of n is also sufficient for odd signature for $t \geq 0$. For $t < 0$, however, the term with alternating sign [Eq. (8)] is typically four orders of magnitude smaller than the term with positive sign throughout, so that more accuracy, and hence more loops, is required. Taking into account the overall accuracy obtainable we have summed up to $n=19$ in these cases.

The extraction of renormalized parameters is illustrated in Fig. 5, for the f and f' at $t=0$.

All amplitudes are divided by s for easier plotting. Both the I_{11}^+ (represented by dots) and the I_{22}^+ (represented by crosses) terms are well fitted by the same power at high s , which then gives directly $\alpha_f(0) = 0.93$. The difference at lower energies between the I_{22}^+ term and its asymptote (represented by pluses) also behaves as a power, which corresponds to the second term in I_{22}^+ , i.e., it gives $\alpha_{f'}(0) = 0.22$. The mixing angle is given by the ratio

$$\lim_{s \rightarrow \infty} I_{22}^+/I_{11}^+ = \tan^2 \theta_f = 0.14 \quad (15)$$

and the coefficient of s^{α_f} is obtained by extrapolating either asymptote to $s = 1$ GeV^2 . For example, we get the value 1.3 for the I_{11}^+ asymptote. Using the calculated value of θ_f we obtain from this $\beta_f = 1.2$. In principle, the same procedure can be repeated to obtain $\theta_{f'}$ and $\beta_{f'}$. However, the difference between I_{11}^+ and its asymptote, even at low s , is too small to give results of any accuracy.²² Notice that the off-diagonal elements have not been used directly. However, their approximate equality is a good check on our calculations.

Repeating the above procedure for the range $-1.0 \leq t \leq 2.3$ we obtain the renormalized f and f' trajectories shown in Fig. 6 (solid curves). The inputs (9) are also shown for comparison. We notice

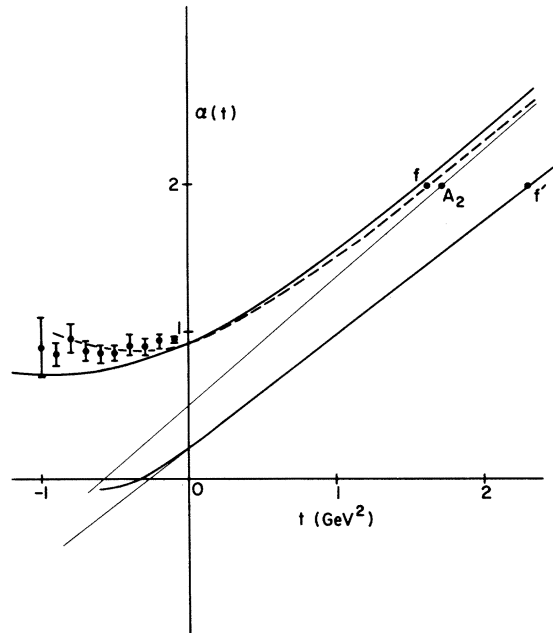


FIG. 6. The renormalized f and f' trajectories, against the inputs $\alpha_{11}(t)$ and $\alpha_{22}(t)$. The physical A_2, f, f' mesons are also shown. The solid curves are obtained with $\kappa_0 = -0.9$ and the dotted curve with $\kappa_0 = -1.3$. The data points are obtained from $\pi^+ p$ elastic scattering (Ref. 26).

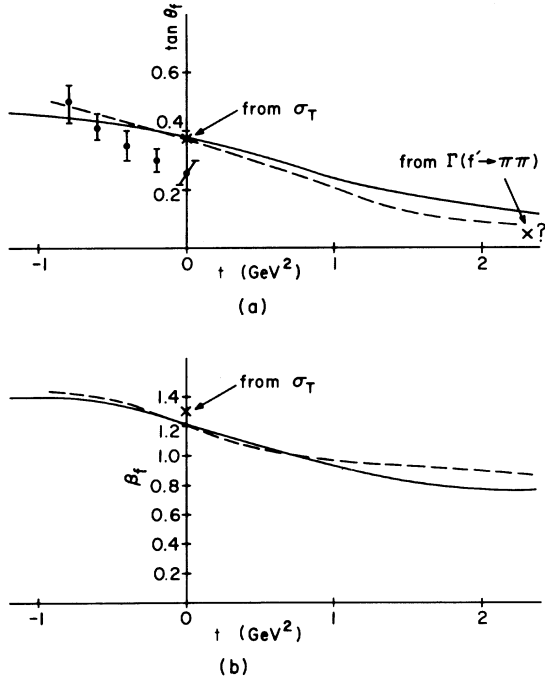


FIG. 7. The variation of (a) $\tan\theta_f$ and (b) β_f as functions of t . The solid curves correspond to $\kappa_0 = -0.9$ and dotted curves to $\kappa_0 = -1.3$. In (a) the data points with marked error bars are from ϕp and ρp elastic amplitudes at 9.3 GeV/c taken from Ref. 30.

immediately that f is considerably renormalized with $\Delta\alpha_f(t)$ decreasing as a function of t . The Regge parameters read from the figure are

$$\alpha_f(0) \approx 0.93, \quad \alpha'_f(0) \approx 0.4, \quad (16)$$

with the trajectory flattening still more for $t < 0$. The slope becomes almost zero around $t \sim -1.0$ (see next section). The f' trajectory, on the other hand, is hardly renormalized at all, especially in the positive t region. It only flattens off slightly for $t < 0$. We obtain for the intercept

$$\alpha_{f'}(0) \approx 0.22. \quad (17)$$

The values of $\tan\theta_f$ are given by the solid curve in Fig. 7(a). θ_f is found to decrease as t increases. Both this behavior and the t dependence of $\Delta\alpha_f$ shown are consistent with the idea that the crossed-loop or cylinder insertion decreases as t increases.^{5,17} Relevant experimental evidence is presented in the next section. The values for β_f are given in Fig. 7(b). In the t range studied, β_f is not very different from unity, showing that the renormalization in the coupling is small.

Similarly, the Regge parameters for the two leading $\sigma = -$ trajectories, named ω and ϕ for convenience, can be obtained from the alternating series (8). However, here one has to be more cau-

tious about accuracy, since the even and odd loops are of comparable size. We believe that most quantities extracted for the ω are still reliable, but things are aggravated for the ϕ , for which one has to take further differences. For instance, we obtain $\alpha_\phi(0) \approx 0$, which we consider to be too low.

The renormalized ω trajectory is shown in Fig. 8. It is apparently somewhat low with an intercept

$$\alpha_\omega(0) \approx 0.36. \quad (18)$$

This, we believe, is because we have neglected baryon exchange, which is known to be sizable and have a positive effect for the ω .²³ Figure 9 gives the variation of $-\tan\theta_\omega$ and β_ω with t (solid curves). Note that $|\tan\theta_\omega|$ falls very fast. The negative sign for $\tan\theta_\omega$ is derived from the off-diagonal elements which are negative.

Of the four zero-quantum-number trajectories studied we are most interested in the f , because it is the highest, and also because it has the same quantum numbers as the vacuum and hence the same as the Pomeron singularity. It is therefore in relation to the f that we want to study phenomenologically the function $\kappa(t)$. From Fig. 6 it is apparent that renormalization effects are not damped fast enough in the sense that the renormalized trajectory "overshoots" the position of the f_0 meson. This is related to the effect mentioned earlier in this section in relation to the triple-Regge vertex. If we insist nonetheless that the trajectory should

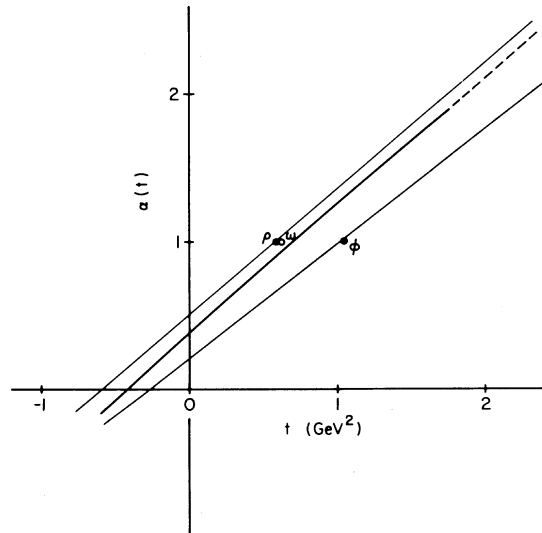


FIG. 8. The renormalized trajectory, against the inputs $\alpha_{11}(t)$ and $\alpha_{22}(t)$. The physical ρ, ω, ϕ mesons are also shown. The solid curve corresponds to $\kappa = -0.9$. The parameterization $\kappa = -1.3$ gives almost identical values, but for a larger range of $t > 0$, where the trajectory is shown by the dotted curve.

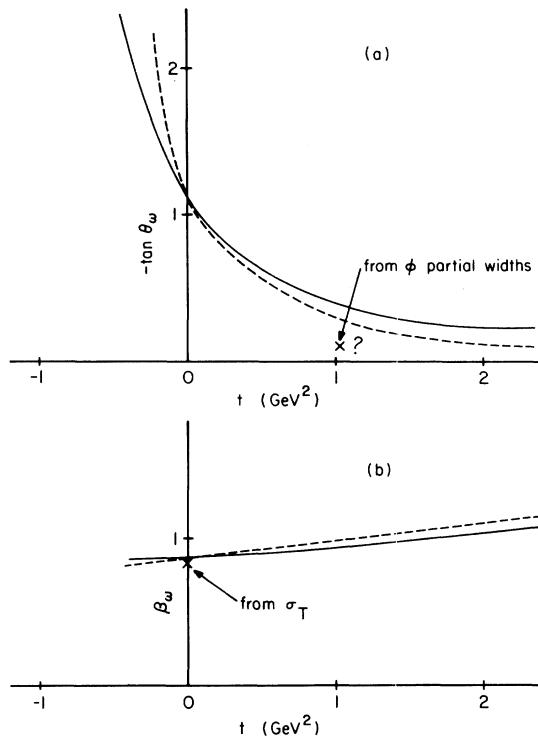


FIG. 9. The variation of (a) $-\tan\theta_\omega$ and (b) β_ω as functions of t . The solid curves correspond to $\kappa_0 = -0.9$ and dotted curves to $\kappa_0 = -1.3$.

pass through the f_0 meson, and if we still keep the linear parameterization (13) as explained earlier, then we obtain

$$\kappa = -1.3. \quad (19)$$

We note in passing that in Ref. 2 two slightly different methods were used for the planar bootstrap, giving two sets of parameters which agree within errors. The two values obtained for κ are identical to (14) and (19). This means that our fitted parameter (19) is still a reasonable value to use within the bootstrap framework.

We repeated the calculations using this fitted value, and the renormalized trajectories $\tan\theta$ and β are shown in Figs. 6 to 9 by dotted curves. They are not qualitatively different from the former curves. Where they actually differ, although slightly, the dotted curves seem to fit the data a little better. For instance, the slope of f at $t=0$ is slightly less at around 0.3, in better agreement with experiment. However, we want to emphasize that the similarities are more significant than the differences. The exercise with (19) shows that although one can do a little better phenomenologically with a more realistic triple-Regge vertex, the bootstrapped values do almost quite as well, with the further advantage, of course, that the param-

eters here are fixed internally. Varying the input trajectories within reasonable bounds also does not change our qualitative picture.¹⁰ We find the stability of our parameters satisfying indeed.

V. COMPARISON WITH DATA

In the system of planar diagrams, there are the exchange degenerate trajectories of the vector-tensor nonet, but there is no Pomeron. The crossed loop introduces diffraction, but as we saw in the preceding sections, no new high-lying trajectory appears. In our method diffraction is generated as the shadow of multiparticle intermediate states, which is also supposed to be the origin of the experimentally observed Pomeron singularity. Now this experimental Pomeron is only known in the region $t \leq 0$, where it has an intercept of about 1 and a small slope of about 0.3. Furthermore, one attributes to it the same quantum numbers as the f . On the other hand, the f trajectory, though exchange degenerate with the ρ at the planar level, lies considerably higher than the other trajectories after renormalization. It now has an intercept of about 0.9 and a slope of about 0.4 at $t=0$. Under these circumstances we think it natural, and compelling if we believe our model at all, to identify this f trajectory with the phenomenological Pomeron.²⁴

The f -Pomeron identity has been much discussed recently. This was first emphasized by Chew and Rosenzweig,⁵ although it was implicit in the earlier work of Chan *et al.*^{1,2} On the basis of an analysis of total cross sections at moderate energies, Stevens, Chew, and Rosenzweig²⁵ concluded that this picture is consistent with experimental data. Since we now have not only the intercept but also the trajectory function within a finite t interval, we are in fact in a stronger position to compare with data. A recent experiment at Fermilab measured several differential elastic-scattering cross sections at laboratory momenta 50, 100, and 200 GeV/ c , in a range of negative t values.²⁶ We took the data at various $-1.0 \leq t \leq -0.1$ and extracted the Pomeron trajectory function from them assuming a single power dependence. The values for π^+p elastic scattering are shown in Fig. 6 and are seen to fall on the renormalized f trajectory within errors. A similar fit is obtained with data for pp elastic scattering. Moreover, Leith in his review²⁷ quoted the following parameters for pp scattering:

$$\begin{aligned} \alpha'_p &= 0.37 \pm 0.08, \quad |t| < 0.1 \text{ GeV}^2, \\ \alpha'_p &= 0.10 \pm 0.06, \quad 0.15 < |t| < 0.5 \text{ GeV}^2. \end{aligned} \quad (20)$$

We obtain respectively 0.29 and 0.09 using (19) and 0.41 and 0.28 using (14), for the same two t ranges.

The quantity β_p is the ratio of the renormalized

f coupling to the bare f coupling; the latter is the same as the bare ρ coupling by construction. At $t=0$, we calculated

$$\beta_f(t=0) \approx 1.2. \quad (21)$$

This can be checked against values obtained from total cross sections. Take for example values at $P_{\text{lab}} = 20 \text{ GeV}/c$:²⁸

$$\begin{aligned} \frac{1}{2}[\sigma_T(\pi^+p) + \sigma_T(\pi^-p)] &= 24.3 \text{ mb} \\ &= \gamma_f^\pi \gamma_f^\rho s^{\alpha_f-1}, \\ \frac{1}{2}[\sigma_T(\pi^-p) - \sigma_T(\pi^+p)] &= 0.8 \text{ mb} \\ &= \gamma_\rho^\pi \gamma_\rho^\rho s^{\alpha_\rho-1}, \\ \frac{1}{2}[\sigma_T(\bar{p}p) + \sigma_T(pp)] &= 43.5 \text{ mb} \\ &= \gamma_f^\rho \gamma_f^\rho s^{\alpha_f-1}. \end{aligned} \quad (22)$$

From these and assuming $\gamma_\rho^\pi = 2\gamma_\rho^\rho$ as in the additive quark model we can deduce immediately

$$\beta_f = \gamma_f^\pi / \gamma_\rho^\pi = 1.3, \quad (23)$$

in fair agreement with the calculated value (21). Similar agreement is obtained for a range of P_{lab} between 40 and 10 GeV/c . We are careful to choose energy ranges before the total cross section rises, where our ideas cannot apply. Incorporating mixing effects at this t value does not affect the approximate agreement of (21) and (23).

The symmetry properties of the renormalized f , as exhibited in the mixing angles, can also be compared to similar quantities derived from experiment. For example, at $P_{\text{lab}} = 10 \text{ GeV}/c$, $\sigma(Kp)/\sigma(\pi p) = 0.77$. Now by simple quark counting,

$$\frac{\sigma(Kp)}{\sigma(\pi p)} = \frac{1}{2}(1 + \sqrt{2} \tan\theta_f),$$

giving $\tan\theta_f = 0.38$, as compared to the calculated value of $\tan\theta_f = 0.38$. Similar agreement is obtained from hyperon cross sections.²⁹ For example, experimentally

$$\frac{\sigma_T(\Lambda p)}{\sigma_T(pp)} \approx 0.87.$$

Now in terms of the mixing angle θ_f ,

$$\frac{\sigma_T(\Lambda p)}{\sigma_T(pp)} = \frac{2}{3} \left(1 + \frac{1}{\sqrt{2}} \tan\theta_f \right),$$

which gives $\tan\theta_f = 0.43$. Similarly the ratio of $\sigma_T(\phi p)$ to $\sigma_T(\rho p)$ also gives an estimate of $\tan\theta_f$. Taking $\sigma_T(\phi p)$ to be 10 to 12 mb and $\sigma_T(\rho p)$ to be 23 to 25 mb, one gets

$$0.3 \leq \tan\theta_f \leq 0.4.$$

Another example deals with $t < 0$. One implication of dual unitarization is that in vacuum exchange amplitudes the singlet component dominates as t

becomes more negative. By taking the eikonal amplitudes instead of the full amplitudes to remove effects of Pomeron-Pomeron cuts, Roberts³⁰ found the above to be true for πN and KN elastic scattering. The ratio of the eikonals for ϕp and ρp at 9.3 GeV/c , taken from Ref. 30, is shown in Fig. 7(a). The uncertainties for this ratio are large (possibly larger than shown), but the general features agree with the behavior of $\tan\theta_f$. However, we must bear in mind that this treatment is model-dependent. The t dependence of our mixing angle is probably not steep enough for t away from the forward direction. This is a reflection of the facts that for t large positive the crossed loop is not damped fast enough, and for t large negative singularities other than the leading poles come into play.

The qualitative, and often quantitative, agreement of the f trajectory with different experimental aspects of the Pomeron appears to us as very convincing for the f -Pomeron identity. We are reminded here of the popularly held idea of f dominance of the Pomeron, first suggested by Carlitz, Green, and Zee,³¹ and exhaustively tested phenomenologically with considerable success by Inami and Roberts.³² Within our scheme this comes automatically, so that the success reported in Ref. 32 also corroborates, though in a weaker sense, the f -Pomeron identity.

We do not have much to say about the renormalized f' trajectory. For $t > 0$, it is almost not renormalized at all, indicating that our original choice of $\alpha_{22}(t)$ to pass through the f' meson was correct. The calculated mixing angle can be compared with the ratio of the partial decay widths of f' into strange and nonstrange mesons. Experimentally it is estimated that³³

$$\frac{\Gamma(f' \rightarrow \pi\pi)}{\Gamma(f' \rightarrow KK)} \approx 0.014. \quad (24)$$

This is related to the angle through

$$\frac{\Gamma(f' \rightarrow \pi\pi)}{\Gamma(f' \rightarrow KK)} = 2 \tan^2\theta_{f'} \times \frac{[q(f' \rightarrow \pi\pi)]^5}{[q(f' \rightarrow KK)]^5} \times \frac{3}{4}, \quad (25)$$

where the numerical factor $\frac{3}{4}$ results from counting spin and quark states. This gives

$$\tan\theta_{f'} \approx 0.05. \quad (26)$$

Since we cannot calculate accurately $\tan\theta_{f'}$, we compare this value to $\tan\theta_f$ in Fig. 7(a). Although as we explained earlier θ_f is not necessarily identical to $\theta_{f'}$, we do expect both to be very small at t large, e.g., at the f' mass. This is clearly borne out by the behavior of $\tan\theta_f$.

Through the crossed-loop insertion, the leading $\sigma = -$ trajectory, which we have called ω for convenience, acquires a considerable admixture of

$\lambda\bar{\lambda}$. This is in contrast to the f trajectory, which remains relatively pure $\mathcal{P}\bar{\mathcal{P}} + \mathcal{K}\bar{\mathcal{K}}$, at least for $t \geq 0$. The coupling β_ω , relative to the ρ , on the other hand, remains fairly stable at 1. These predictions can all be tested against experiment. A recent analysis³⁴ of total cross-section data gives the following couplings:

$$\gamma_{KK}^\rho = 1.14 \text{ (mb)}^{1/2}, \quad \gamma_{KK}^\omega = 1.63 \text{ (mb)}^{1/2}, \quad (27)$$

giving the ratio

$$\gamma_{KK}^\omega / \gamma_{KK}^\rho = 1.4. \quad (28)$$

From Fig. 7 we read off

$$\tan\theta_\omega(t=0) \simeq -1.1, \quad \beta_\omega(t=0) \simeq 0.9,$$

which give the ratio

$$\gamma_{KK}^\omega / \gamma_{KK}^\rho = \beta_\omega (\cos\theta_\omega - \sqrt{2} \sin\theta_\omega) \simeq 1.5, \quad (29)$$

agreeing well with (28).

On the other hand, we know that our picture of the ω cannot be complete. Using a one-dimensional model, Chan and I⁷ have shown that the effect of baryon exchange is non-negligible at $t=0$ for ω . Preliminary results of Hansson¹² are similar. Now baryon exchange has the effect of renormalizing both signatures by a positive amount—much smaller for the f than for the ω . This effect, if incorporated in our present calculations, would push up the ω trajectory, taking the intercept nearer to the phenomenological estimate of 0.43.³⁴

Figures 8 and 9 for the ω parameters are given with a smaller $t < 0$ range. This is because of the difficulties we mentioned in Sec. IV. In the positive t region, where $\alpha_f - \alpha_\omega$ is not so large, the terms I^- are still not too small compared to I^+ . In other words, the accuracy in the ω parameters is still not much impaired by taking differences. Unfortunately this is no longer the case for $t < 0$. As t becomes more negative, α_ω goes farther and farther away from α_f , with the result that I^- is four or five orders of magnitude down from I^+ (in the t region considered). Also, other effects come into play. In the first place, at such low values of α the leading-pole assumption certainly breaks down. We know that low-lying complex poles^{4,7} are present, whose effect will no longer be negligible here. The slightly oscillatory behavior of our results is a possible indication of this. Furthermore, the term I_{11}^- seems to go through zero somewhere between $t = -0.3$ and $t = -0.5$.³⁵ We doubt, however, that this has to do with the cross-over zero near $t = -0.2$. These features can probably be further

elucidated by more detailed analysis of our numerical results. However, because of the necessarily restricting approximations we made for our model, we have no way to estimate whether these features reflect the real nature of the ω .

Similar remarks apply to the ϕ trajectory with even greater poignancy. We obtain the ϕ intercept to be around 0, which at first sight seems to be rather low. However, Chew and Rosenzweig⁵ arrived at a similar low value using a one-dimensional model. The value of the mixing angle can be compared with the partial decay widths of ϕ . We have

$$\frac{\Gamma(\phi \rightarrow \rho\pi)}{\Gamma(\phi \rightarrow K\bar{K})} = 2 \tan^2\theta_\phi \times \frac{[q(\phi \rightarrow \rho\pi)]^3}{[q(\phi \rightarrow K\bar{K})]^3} \times \frac{12}{4}. \quad (30)$$

Equating this with the experimental value of 0.20, we obtain

$$|\tan\theta_\phi| = 0.1. \quad (31)$$

As with the f' meson, we try to compare this with $\tan\theta_\omega$ at the ϕ mass in Fig. 9(a). Although this comparison is quantitatively inconclusive due to the possible difference between θ_ω and θ_ϕ , the dramatic decrease of $|\tan\theta_\omega|$ from above 1 at $t \sim 0$ to less than 0.3 at the ϕ mass shows that one can expect the two quantities to be closely related.

In conclusion we think that the agreement with data is satisfactory where such comparison is possible. In particular, our picture of the renormalized vacuum trajectory f can account for most data at moderate energies without introducing an extra singularity with similar intercept. After renormalization our ω trajectory acquires a significant admixture of the strange component, which is borne out by experimental estimates. However, a complete description of the ω should include the baryon exchanges as well, which we are unable yet to incorporate into our scheme with three-dimensional kinematics. Besides these comparisons with existing data, our model has definite predictions about the trajectory functions, couplings, and mixing properties for a range of t which have yet to be tested.

ACKNOWLEDGMENTS

I would like to thank C. Rosenzweig for useful correspondence, T. H. Hansson for showing me his results prior to publication, and Chan Hong-Mo for critically reading the manuscript. Also I wish to thank Professor C. N. Yang and his colleagues for their hospitality at the Institute for Theoretical Physics.

- *Research partially supported by the National Science Foundation under Grant No. PHY 76-15328.
- †On leave from Department of Theoretical Physics, University of Oxford.
- ¹Chan Hong-Mo, J. E. Paton, and Tsou Sheung Tsun, Nucl. Phys. B86, 479 (1974).
- ²Chan Hong-Mo, J. E. Paton, Tsou Sheung Tsun, and Ng Sing Wai, Nucl. Phys. B92, 13 (1975).
- ³J. P. Aurenche *et al.*, paper delivered by J. E. Paton, in Proceedings of the Vth Colloquium on Multiparticle Reactions, Oxford (unpublished); Chan Hong-Mo and Tsou Sheung Tsun (review paper), Rutherford Laboratory Report No. RL-76-080, 1976, to be published in the Proceedings of the Summer Institute at Bielefeld, 1976.
- ⁴N. Sakai, Nucl. Phys. B99, 167 (1975).
- ⁵G. F. Chew and C. Rosenzweig, Phys. Lett. 58B, 93 (1975); Phys. Rev. D 12, 3907 (1975).
- ⁶C. Schmid and C. Sorensen, Nucl. Phys. B96, 209 (1975); N. Papadopoulos, C. Schmid, C. Sorensen, and D. Webber, *ibid.* B101, 189 (1975).
- ⁷Chan Hong-Mo and Tsou Sheung Tsun, Nucl. Phys. B118, 413 (1977).
- ⁸M. Bishari, Phys. Lett. 59B, 461 (1975).
- ⁹J. Finkelstein and J. Koplík, Phys. Rev. D 14, 1437 (1976).
- ¹⁰Tsou Sheung Tsun, Phys. Lett. 65B, 81 (1976).
- ¹¹Louis Balázs, Phys. Rev. D 15, 309 (1977).
- ¹²T. H. Hansson, work in preparation.
- ¹³J. Kwiecinski and N. Sakai, Nucl. Phys. B106, 44 (1976).
- ¹⁴G. Veneziano, Phys. Lett. 52B, 220 (1974); Nucl. Phys. B74, 365 (1974); M. Ciafaloni, G. Marchesini, and G. Veneziano, *ibid.* B98, 472 (1975); B98, 493 (1975).
- ¹⁵Chan Hong-Mo, Ken-ichi Konishi, J. Kwiecinski, and R. G. Roberts, Phys. Lett. 63B, 441 (1976).
- ¹⁶G. F. Chew and C. Rosenzweig, Phys. Rev. D 15, 3433 (1977).
- ¹⁷Chan Hong-Mo, K. Konishi, J. Kwiecinski, and R. G. Roberts, Phys. Lett. 64B, 301 (1976).
- ¹⁸This is not exactly the case here. Because of approximations made in deriving Eq. (5), the amplitude still depends on the external masses, though weakly. For simplicity we set them equal to zero here. (See Ref. 2).
- ¹⁹For the intercepts this was proved by Papadopoulos *et al.* (Ref. 6) and Konishi (Ref. 20) using simplified arguments.
- ²⁰K. Konishi, Nucl. Phys. B116, 356 (1976).
- ²¹J. E. Dodd, Nucl. Phys. B119, 334 (1977).
- ²²If we did pursue this, we would obtain $\tan\theta_{f_1}(0) \approx 1$ and $\beta_{f_1}(0) \approx 1$ from Fig. 5.
- ²³See Sec. V and Refs. 7 and 12.
- ²⁴Here it is of course not a question of whether there exist any additional high-lying singularities at asymptotic energies, such as that conceived in the dual resonance model and gluon theory, which might also be called the Pomeron. We are concerned here only with the Pomeron that issues from fitting data at non-asymptotic energies, such as currently done in Regge phenomenology.
- ²⁵P. Stevens, G. F. Chew, and C. Rosenzweig, Nucl. Phys. B110, 355 (1975).
- ²⁶C. W. Akerlof *et al.*, Phys. Rev. D 14, 2864 (1976).
- ²⁷D. W. G. S. Leith, in *The Strong Interactions*, SLAC Summer Institute on Particle Physics, 1974, edited by M. C. Zipf (National Technical Information Service, U. S. Dept. of Commerce, Springfield, Virginia, 1974), Vol. 1.
- ²⁸A. S. Carroll *et al.*, Phys. Lett. 61B, 303 (1976).
- ²⁹A. N. Diddens, in *Proceedings of the Fourth International Conference on High Energy Collisions, Oxford*, 1972, edited by J. R. Smith (Rutherford High Energy Laboratory, Chilton, Didcot, Berkshire, England, 1972).
- ³⁰R. G. Roberts, Nucl. Phys. B116, 334 (1977).
- ³¹R. Carlitz, M. Green, and A. Zee, Phys. Rev. D 4, 3439 (1971).
- ³²T. Inami and R. G. Roberts, Nucl. Phys. B93, 497 (1975).
- ³³A. J. Pawlicki *et al.*, Phys. Rev. Lett. 37, 971 (1976).
- ³⁴R. E. Hendrick *et al.*, Phys. Rev. D 11, 536 (1975).
- ³⁵The behavior of $\tan^2\theta_\omega = \lim(I_{22}^2/I_{11}^2)$ indicates a discontinuity somewhere in this interval. The rapid rise in Fig. 9(a) shows one side of this discontinuity.